Received: 21 November 2019 | Accepted: 1 June 2020

DOI: 10.1002/vzj2.20048

Vadose Zone Journal

ORIGINAL RESEARCH ARTICLES

Determination of the relative macroporosity and the effective aggregate width for different macropore geometries with disk infiltrometers

C. A. Faúndez Urbina[1,3] | **J. C. van Dam**[1] | **F. van den Berg**[2] | **C. J. Ritsema**[1] | **D. W. S. Tang**[1]

[1] Soil Physics and Land Management Group, Wageningen Univ. & Research, PO Box 47, Wageningen 6700AA, the Netherlands

[2] Wageningen Environmental Research, PO Box 47, Wageningen 6700AA, the Netherlands

[3] Institution de Ciencias Agroalimentarias, Animales y Ambientales, Univ. de OHiggins, Ruta 90 Kilómetro 3, San Fernando, Chile

Correspondence
C. A. Faúndez Urbina, Soil Physics and Land Management Group, Wageningen Univ. & Research, PO Box 47, 6700 AA, Wageningen, the Netherlands.
Email: carlos.faundezurbina@wur.nl

Funding information
Fondo de Fomento al Desarrollo Científico y Tecnológico, Grant/Award Numbers: Doctorado Becas Chile/2015, -, 72160322

Abstract

The relative macroporosity (w_f) and the effective aggregate width (d_{ag}) are input parameters for several dual-permeability models. As w_f is geometrically related to d_{ag}, any improvement in its determination is directly extended to d_{ag}. The w_f, as estimated by disk infiltrometers, applies only under the assumption that macropores are cylindrically shaped. We generalize the determination of w_f for ring, hexagon, brick, and rectangular slab macropore-matrix shapes using a transformation factor, ξ, obtained from pore-scale modeling. The ξ was computed by dividing the relative macroporosity for noncylindrical shapes, w_{f_nc}, over the relative macroporosity for cylindrical shapes, w_{f_c}. The computation of ξ accounts for differences in the macropore area and macropore water flow between noncylindrical and cylindrical shapes. A total of 15 combinations of macropore width and effective aggregate width were used to construct the geometrical figures and compute both w_{f_nc} and w_{f_c}. For the cylindrical, ring, and rectangular slab shapes, the macropore water flow was solved using analytical solutions. For the hexagonal and brick shapes, the macropore water flow was solved numerically using COMSOL Multiphysics. Remarkably, the computed ξ was constant and equal to 1.5 for all four noncylindrical shapes under analysis. We show that the solution is exact for laminar flow under saturated conditions in the macropores with a rigid and wettable matrix. This methodology enables the derivation of a better estimate of w_f and d_{ag} from disk infiltrometer data that include different macropore geometries. This information is crucial for the setup of dual-permeability models in risk assessments and detailed studies.

1 | INTRODUCTION

A Richards-based dual-permeability model requires solving matrix and macropore water flow separately, then coupling them with lateral mass transfer equations (Gerke & van Genuchten, 1993a, 1993b). Excellent performance of dual-permeability models was reported in laboratory studies, demonstrating the validity of the concept (Arora, Mohanty, & McGuire, 2011; Köhne & Mohanty, 2005). Under field conditions, dual-permeability models have

been used for simulating water flow and chemical transport in drainage systems (Gardenas, Simunek, Jarvis, & van Genuchten, 2006; Scorza Júnior, Jarvis, Boesten, van der Zee, & Roulier, 2007; Tiktak, Hendriks, Boesten, & van der Linden, 2012) and water redistribution in semiarid environments (van Schaik, Hendriks, & van Dam, 2010). Therefore, dual-permeability models are an essential component of agricultural and environmental studies involving the computation of water and chemical mass balances. A large number of parameters, however, may discourage the use of dual-permeability models, especially because some parameters are difficult to measure in the field.

Parameterization of dual-permeability models is a difficult task, and it is considered relevant for further research (Van den Berg, Gottesbüren, Hammel, Jarvis, & Poot, 2014). A complete parameterization of dual-permeability models is essential for both local- and regional-scale studies. One possible approach is to obtain high-quality data to be used in parameter estimation by inverse methods (e.g., Andelst study; Scorza Júnior, Smelt, Boesten, Hendriks, & van der Zee, 2004). This methodology provides sufficient estimates for local studies, but the large data requirements and computational burden render it impractical for regional studies. Furthermore, inverse methods require reasonable initial estimates of dual-permeability model parameters and uncertainty bounds for computational efficiency (Arora et al., 2011; Köhne, Köhne, & Gerke, 2002). Therefore, the ability to roughly estimate dual-permeability model parameters is essential, regardless of whether more precise estimations are to be obtained through inverse methods. Additionally, it is pertinent for risk assessment or regional studies, where the availability of data for calibration is scarce.

The effective aggregate width (d_{ag}) and the relative macroporosity (w_f) are common input parameters for dual-permeability models. The d_{ag} denotes the characteristic distance from the macropore wall to the center of the matrix. The distance is measured parallel to the soil surface in different cross-sectional planes over depth. The w_f refers to the total area (or volume) of macropores over a reference area (or volume) of soil. The d_{ag} is mathematically related to w_f (see Section 2). Therefore, any improvement in the determination of w_f is directly passed on to d_{ag}. The last point is essential because d_{ag} has typically been estimated by calibration or pedotransfer functions under field conditions (Scorza Júnior et al., 2007; Tiktak, Hendriks, & Boesten, 2012). Therefore, alternative methods for an independent determination of d_{ag} and w_f under field conditions are useful.

Accurate estimations of d_{ag} have been performed under controlled laboratory conditions using cylindrical macropores surrounded by a cylindrical matrix mantle (Arora et al., 2011; Urbina et al., 2019). These conditions allow precise knowledge of w_f, the effective macropore width, b_e, and the macropore-matrix shape over depth. The b_e is defined here as the half-radius of a cylindrical macropore or, for other shapes, some characteristic macropore half-width. Accurate determinations of d_{ag}, w_f, and b_e under field conditions can be performed by computed tomography (Hu, Feng, Yang, & Wang, 2014; Zhang, Xu, Li, Hou, & Ren, 2017). However, this technology is not widely available to institutions worldwide. Alternatively, w_f and b_e can be estimated by disk infiltrometers under field conditions. Those values, along with the macropore-matrix shape, can be used to approximate d_{ag}.

Disk infiltrometers allow for the determination of d_{ag}, w_f, and b_e only under the assumption of cylindrical macropores and quasi-steady-state one-domain flow conditions (Watson & Luxmoore, 1986). The use of disk infiltrometers to obtain d_{ag}, w_f, and b_e in noncylindrical macropore-matrix shapes is challenging and is a limitation of the methodology. Noncylindrical macropore-matrix shapes include rings, hexagons, bricks, and rectangular slabs. Those shapes have already been incorporated into various dual-permeability models (e.g., Gerke & van Genuchten, 1996). Therefore, the challenge is to generalize the computation of d_{ag} and w_f for noncylindrical macropore-matrix geometries with disk infiltrometers.

The main objective of this research was to compute a transformation factor (ξ) for the estimation of the relative macroporosity, w_f, in the ring, hexagon, brick, and rectangular slab macropore-matrix shapes under laminar flow conditions. A mathematical and geometrical relation between d_{ag} and w_f for different macropore-matrix shapes is explicitly shown in Section 2. Implications of ξ in the computation of d_{ag} are also presented in Sections 2 and 5. The outcomes of this research will allow for the generation of a theoretical estimate of the effective aggregate width, d_{ag}, and the relative macroporosity, w_f, for noncylindrical and cylindrical geometries, using disk infiltrometers.

Core Ideas

- The relative macroporosity and effective aggregate width are mathematically related.
- The transformation factor is constant for noncylindrical shapes.
- Computation of the relative macroporosity for mixed geometries is included.
- HYDRUS, MACRO, and SWAP models can be parameterized with this methodology.
- The methodology can be applied to existing disk infiltrometer databases.

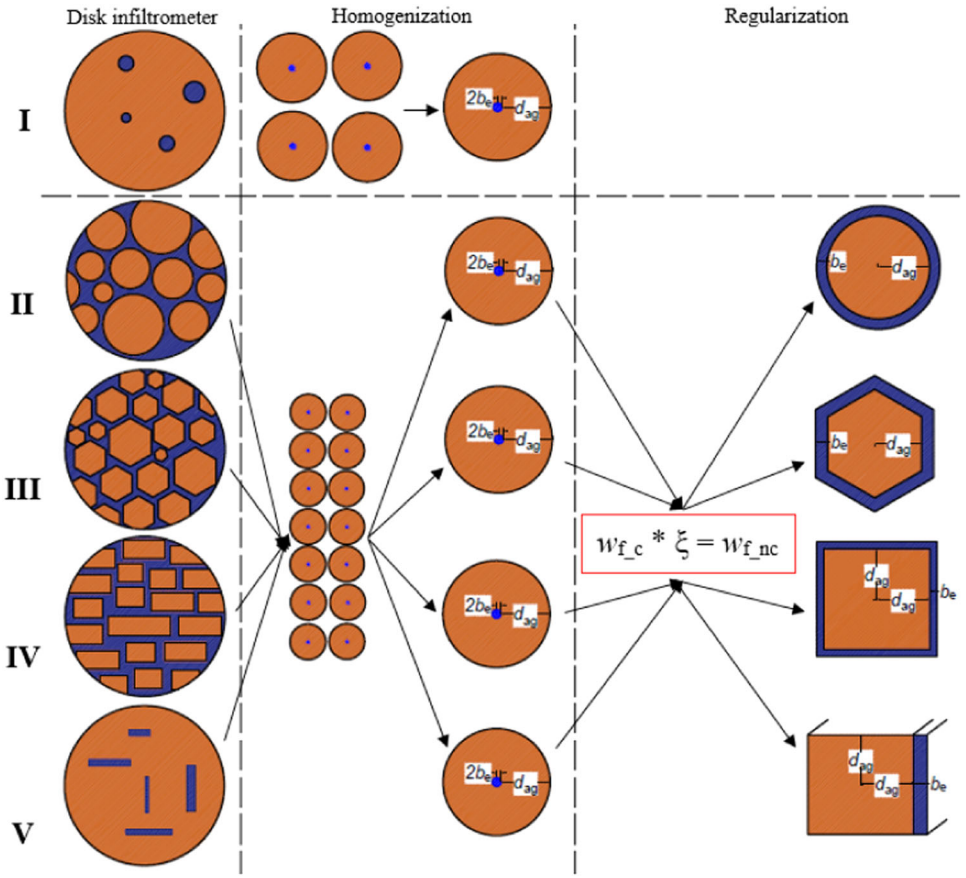

FIGURE 1 Schematic representation of a disk infiltrometer measurement for cylinders (I), rings (II), hexagons (III), bricks (IV), and rectangular slabs (V). The homogenization and regularization steps are applied to obtain d_{ag} and w_f for noncylindrical shapes. b_e is the effective macropore width; d_{ag} is the effective aggregate width; $w_{f\_c,}$ and w_{f_nc} are the relative macroporosities for cylindrical and noncylindrical shapes, respectively; and ξ is the transformation factor

2 | THEORETICAL FRAMEWORK

In this section, relevant physical concepts and the introduction of the novel transformation factor is included. The concept of "porous block" is commonly used in this manuscript; hence, it is crucial to know its definition. A porous block is an idealized geometrical figure formed by a macropore and its corresponding matrix. This term was used similarly in Gerke and van Genuchten (1996). An example of a cylindrical porous block is found in Figure 1, "Homogenization." The cylindrical porous block is formed by a cylindrical macropore of radius = $2b_e$ and its matrix mantle of width = d_{ag}. The matrix mantle is the soil matrix between the macropore wall and the limit of the porous block. Four types of noncylindrical porous blocks are found in Figure 1, "Regularization." For example, the brick shape porous block is formed by the half-width of the macropore (b_e) and its inner matrix, including a half-width = d_{ag}.

The computation of the transformation factor, ξ, compares the four noncylindrical porous blocks against the cylindrical porous block, as is depicted in Figure 1, "Regularization." It is worth to mention that in Gerke and van Genuchten (1996), the cylindrical macropore surrounded by a cylindrical matrix mantle is denoted as a "hollow cylinder," whereas the ring porous block is denoted as "solid cylinder."

2.1 | Young–Laplace capillarity theory

For water at 20 °C and a contact angle of zero between the liquid–vapor–solid interface, the equivalent macropore radius (r_m, cm) for a given pressure head (h) is

$$r_m \cong \frac{-0.15}{h} \text{ cm}; \quad r_m = 2b_e \tag{1}$$

where h (cm) is the pressure head imposed at the base of the disk infiltrometer. For macropore shapes other than cylindrical and spherical, the following solution of

Young–Laplace for parallel plates can be used:

$$d_T \cong \frac{-0.15}{h} \text{ cm}; \quad d_T = 2\, b_e \tag{2}$$

where d_T (cm) is the width between two parallel plates (or matrix walls). The fixed pressure head employed at the base of the disk infiltrometer determines the effective macropore radius (Equation 1) or effective macropore width (Equation 2), above which a macropore is excluded from the water flow process. We advise using Equation 2 instead of Equation 1 for noncylindrical geometries as an approximation of the macropore width.

2.2 | Relative macroporosity

The relative macroporosity is obtained by dividing the total macropore area (m^2) over the total surface area of infiltration (A_R, m^2) as follows:

$$w_f = \frac{N A_m}{A_R} \tag{3}$$

where N is the number of macropores, and A_m (m^2) is the average macropore cross-sectional area. Equation 3 can be modified as follows:

$$w_f = A_m \left(\frac{A_R}{N}\right)^{-1} \tag{4}$$

where A_R over N is the average area of a porous block; therefore, the union of the macropore and its matrix area. Equations 3 and 4 can be used for any geometry. Practitioners should be aware that A_R can be the total surface area of infiltration of a disk infiltrometer or the total surface area of infiltration of a noncylindrical porous block (see the computation of the transformation factor in Section 3).

2.3 | Number of macropores

The number of macropores of a given size (i.e., r_m or d_T) can be obtained by

$$N = \frac{Q}{q} \tag{5}$$

where Q ($m^3\ s^{-1}$) and q ($m^3\ s^{-1}$) are water flow rate, and the meaning of those water flow rates is context dependent, because Equation 5 is used for different situations in this paper. Q may be the water flow rate from a disk permeameter under a given pressure head (see Equations 1 and 2), and q may be the water flow rate computed for the macropore by pore-scale simulation.

2.4 | The effective aggregate width

The effective aggregate width is computed from a cylindrical or noncylindrical porous block. The w_f and the effective macropore width (b_e) are input parameters for obtaining the effective aggregate width, d_{ag}, for different porous blocks, as follows:

$$d_{ag} = 2b_e \left[\frac{1}{(w_{f\_c})^{1/2}} - 1\right] \tag{6}$$

where w_f]0,1] (cylindrical shapes);

$$d_{ag} = \frac{b_e}{\left\{\left[1 - (w_{f\_c} \cdot \xi)\right]^{-1/2} - 1\right\}} \tag{7}$$

where w_f]0,1[(rings, hexagons, and bricks);

$$d_{ag} = b_e \left[\frac{1}{(w_{f\_c} \cdot \xi)} - 1\right] \tag{8}$$

where w_f]0,1] (rectangular slabs);

where d_{ag} is the width of the cylindrical matrix mantle in Equation 6, the radius of the ring matrix or the half-width for the brick matrix or the apothem for the regular hexagon matrix in Equation 7, and the half-width of the rectangular slab matrix in Equation 8. The b_e is the half-radius of the macropore in Equation 6 and is the macropore half-width in Equations 7 and 8, and w_{f_c} is the relative macroporosity for cylindrical shapes. The ξ was previously defined. Some of these equations were derived from Gerke and van Genuchten (1996). Equations 6–8 demonstrates the mathematical relation between d_{ag} and w_f for different geometries. Next, we will show how to approximate w_f and b_e for noncylindrical shapes with a disk infiltrometer, to subsequently approximate d_{ag} using Equations 7 and 8.

2.5 | Disk infiltrometer

The disk infiltrometer is a device that allows for the measurement of infiltration rates at different pressure heads imposed at the base of a disk (Perroux & White, 1988). These pressure heads can be transformed into a macropore radius (Equation 1) or macropore width (Equation 2) using the Young–Laplace capillarity theory. Therefore, the above equations (Equation 3–8) can be applied to different

pressure heads if a threshold for differentiating between the macropores and the matrix system is set. Based on experimental evidence, Jarvis (2007) suggested the threshold value be −10 or −6 cm pressure head for use in Equations 1 and 2.

Two example cases are presented below. In Case 1, we explain how d_{ag} and w_f could be computed from disk infiltrometers for cylindrical shapes. In Case 2, we show the limitations of the use of disk infiltrometer for the obtainment of d_{ag} and w_f for noncylindrical shapes.

2.5.1 | Case 1: Disk infiltrometers and cylindrical shapes

Let us assume a field condition where four cylindrical macropores of a radius ≥0.06 cm are found (Figure 1, I). Placing the disk at 0 and −3 cm pressure head allows us to measure the macropore water flux in that pressure head range as follows:

$$q_{D[0,-3]} = \frac{Q_0 - Q_3}{A_R} \tag{9}$$

where $q_{D[0,-3]}$ is the water flux displaced by the disk infiltrometer (m s^{-1}) for the pressure head range [0, −3], Q_0 is the water flow displaced by the disk infiltrometer at 0 pressure head (m^3 s^{-1}), and Q_3 is the water flow displaced by the disk infiltrometer at −3 cm pressure head (m^3 s^{-1}). The minimum macropore radius that transports water in $q_{D[0,-3]}$ is obtained by substituting −3 cm in Equation 1, which results in $r_m = 0.05$ cm.

The number of cylindrical macropores, N_c, can be obtained by applying Darcy's law (the numerator in Equation 10) and the Hagen–Poiseuille equation (the denominator in Equation 10), assuming quasi-steady-state laminar flow conditions (Dunn & Phillips, 1991; Watson & Luxmoore, 1986), the outcome of which was

$$N_{c[0,-3]} = \frac{q_{D[0,-3]} A_R 8\eta}{\pi \rho g r^4_{m,-3}} \tag{10}$$

where η is the dynamic viscosity of water (kg m^{-1} s^{-1}), ρ is the density of water (kg m^{-3}), g is the gravitational constant (m s^{-2}), and $r_{m,-3}$, is 0.05 cm for $h = -3$ cm. The derivation of Equation 10 can be found in the supplemental material. The primary assumption in Equation 10 is one-domain flow conditions that produce a unitary gradient. Hence, the saturated hydraulic conductivity from Darcy (K) is equal to q_D.

The average macropore cross-sectional area of the cylindrical porous block (A_m in Equations 3 and 4) is computed by setting $r_m = 0.05$ cm as the radius. The computation of d_{ag} requires choosing the shape of the porous block. Recall that in this case, the macropore shape is cylindrical, and for practical applications, we set a cylindrical matrix mantle. Therefore, the equations below for w_f (Equation 3) and d_{ag} (Equation 6) are valid for a cylindrical porous block:

$$w_{fc[0.-3]} = \frac{N_{c[0,-3]} A_{m,-3}}{A_R} \tag{11}$$

$$d_{ag[0,-3]} = 2b_{e,-3}\left[\frac{1}{\left(w_{fc[0,-3]}\right)^{1/2}} - 1\right] \tag{12}$$

where the subscript [0, −3] means that the variable was computed for that pressure head range, and the subscript −3 (in A_m and b_e) means that those variables were computed with the corresponding maximum macropore radius involved in the infiltration process (0.05 cm). Recall that $b_e = 0.025$ cm in Equation 12 (half-radius).

Practitioners should notice that the assumption of a cylindrical porous block for the computation of d_{ag} is just a conceptualization. Hence, the matrix surrounding the cylindrical macropore can be different (e.g., squared matrix). However, cylindrical macropores and cylindrical matrix mantle have been applied in previous research with dual-permeability models for the obtainment of d_{ag} and w_f (Arora et al., 2011; Urbina et al., 2019). Therefore, it is convenient to keep that conceptualization. Previous settings imply that the four cylindrical porous block areas do not fit below the disk infiltrometer area. That issue occurs because the conceptualization performed here looks to keep the relative macroporosity constant between the porous blocks. This conceptualization is one of the characteristics of homogenization (Figure 1).

Homogenization is based on Equation 11 for w_f (Figure 1, "Homogenization"). We observed that Equation 11 (see Equation 4) implies that the total surface area of infiltration (A_R) is being divided by the number of macropores (N). Therefore, using the previous example, four individual porous blocks are generated by homogenization. Every porous block contains a cylindrical macropore of radius 0.05 cm, and they contain the same matrix area, which is conceptualized as a cylindrical matrix mantle. Thus, the four porous blocks have the same d_{ag} and w_f. A result of homogenization is that the w_f computed using the four macropores over the disk infiltrometer area by Equation 11 must be the same as that computed for an individual porous block using Equation 4. Additionally, the water flow transported by all the porous blocks is the same as the displaced water by the disk infiltrometer (see Equation 10). Regularization (Figure 1) is not applied to cylindrical macropores shapes.

Previous computations in Equations 11 and 12 indicate that both d_{ag} and w_f must be computed for more pressure head ranges until the threshold of −10 cm pressure head is achieved. Additionally, including more pressure head ranges reduces the error associated with homogenization (Figure 1, I). Understanding homogenization is critical because it is the base of the estimation of d_{ag} and w_f for noncylindrical geometries.

2.5.2 | Case 2: Disk infiltrometers and noncylindrical shapes

The average macropore cross-sectional area (and thus w_f) for noncylindrical shapes (Figure 1, II–V) cannot be computed using disk infiltrometers because more than one dimension is required (in cylindrical cases, only the radius is needed to compute the average macropore cross-sectional area). We generate a three-step process that includes the homogenization and regularization steps in order to compute the relative macroporosity for noncylindrical shapes, w_{f_nc} (Figure 1).

Let us consider infiltrated water measured by disk infiltrometer in a pressure head range of [0, −3], and that the macropore width, d_T, is computed by Equation 2 setting $h = -3$ cm. The first step is to observe the macropore-matrix shape under field conditions where the disk infiltrometer is to be applied. The second step is to presume that the infiltrated water is transported by a bundle of cylindrical porous blocks (Figure 1, II-V, "Homogenization"), where each cylindrical macropore in a cylindrical porous block has a radius equal to the macropore width or $r_m = d_T = 2b_e = 0.05$ cm (see Equations 1 and 2). From the bundle of cylindrical porous blocks, we compute an incorrect w_f following the methodology of Case 1. To rectify w_f, we apply the regularization step, which is the third step. Regularization implies the use of the relative macroporosity of a cylindrical porous block (w_{f_c}) multiplied by a transformation factor, ξ, to obtain the relative macroporosity for the noncylindrical porous block (w_{f_nc}) that was initially observed under field conditions (Figure 1, I–IV, "Regularization"). Therefore, the transformation factor, ξ, is defined as the ratio between w_{f_nc} and w_{f_c}, and is only applied in the regularization step for noncylindrical shapes (Figure 1). Computing the transformation factor, ξ, is the objective of this research.

The effective aggregate width, d_{ag}, can now be computed for different macropore-matrix shapes because we can compute the relative macroporosity of noncylindrical shapes following the abovementioned methodology. The relative macroporosity for cylindrical shapes w_{f_c} along with ξ can be set in Equations 7 or 8 to compute d_{ag}. Care should be taken to use the half-width of the macropore in Equations 7 or 8. In the previous example where $d_T = 0.05$ cm (macropore width), $b_e = 0.025$ cm (macropore half-width for noncylindrical shapes).

To simplify the analysis, a regular hexagon represents the irregular hexagon after regularization, where the apothem of the regular hexagon is d_{ag}. A square shape represents bricks and rectangular slab shapes, to have a unique d_{ag} after regularization (Figure 1, IV and V, "Regularization").

3 | METHODS

The computation of the transformation factor explained below is illustrated comparing one noncylindrical porous block against one cylindrical porous block. Therefore, we include homogenization and regularization from Figure 1, II–IV.

3.1 | Transformation factor

The transformation factor, ξ, is the ration of the relative macroporosity of a noncylindrical porous block (w_{f_nc}) against the relative macroporosity of a cylindrical porous block (w_{f_c}) as follows:

$$\xi = \frac{w_{f\_nc}}{w_{f\_c}} \tag{13}$$

$$\xi = \frac{\left(N_{nc}A_{m\_nc}/A_R\right)}{\left(N_cA_{m\_c}/A_R\right)} = \frac{A_{m\_nc}q_c}{A_{m\_c}q_{nc}} \tag{14}$$

where the subscripts "nc" and "c" at each variable mean noncylindrical and cylindrical shapes, respectively, and q is macropore water flow. The left-hand side of Equation 14 was derived from Equation 3 for w_f. The right-hand side of Equation 14 was obtained by setting the noncylindrical porous block as the reference shape, hence the number of noncylindrical porous blocks is one ($N_{nc} = 1$). Therefore, in this setting, the total surface area of infiltration, A_R, is equal to the area of the noncylindrical porous block (matrix and macropore area).

The number of cylindrical shapes, N_c, is different from one, and it is computed using Equation 5 where Q means the macropore water flow of the noncylindrical porous block (reference), q_{nc}, and q means the macropore water flow of the cylindrical porous block, q_c. In simple terms, the meaning of N_c is the amount of cylindrical porous block necessary to transport the same amount of water as the reference noncylindrical porous block. Hence, the transformation factor ξ accounts for differences in the macropore area and macropore water flow between noncylindrical and cylindrical shapes.

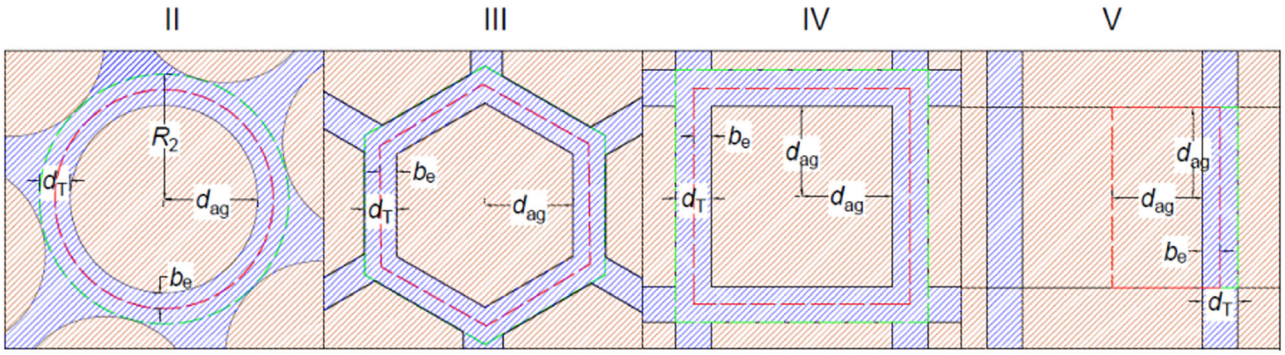

FIGURE 2 The dashed red line depicts the boundary of the noncylindrical porous block, including the effective macropore width, b_e, and the effective aggregate width, d_{ag}. The dashed green line depicts the outer border of the macropore area where the water flow computations take place, including the macropore width, d_T. This water flow is divided by two to match the boundaries of the noncylindrical porous block. Outer radius $R_2 = d_{ag} + d_T$ (Equation 20). The roman numerals follow the order of Figure 1: rings (II), hexagons (III), bricks (IV), and rectangular slabs (V)

To quantify ξ, we generated 15 geometrical figures for rings, hexagons, bricks, and rectangular slabs combining three macropore widths, d_T (0.075, 0.050, and 0.025 cm), and five effective aggregate widths, d_{ag} (0.5, 1.25, 2.5, 3.75, and 5.0 cm). The radius of the transitional cylindrical porous block was set as $d_T = 2b_e$ (homogenization and regularization step in Figure 1). Previous information is enough to compute w_{f_nc} and w_{f_c} and thus the transformation factor by Equations 13 and 14. An example of the construction of the macropore-matrix shapes is presented in the supplemental material.

3.1.1 | Average macropore cross-sectional area

The average macropore cross-sectional area, A_m, is needed in Equation 14. We computed A_m for rings (Equation 15), hexagons (Equation 16), bricks (Equation 17), and rectangular slabs (Equation 18) as follows:

$$A_{m\_nc} = \pi\left[\left(d_{ag} + b_e\right)^2 - {d_{ag}}^2\right] \quad (15)$$

$$A_{m\_nc} = 2\sqrt{3}\left[\left(d_{ag} + b_e\right)^2 - d_{ag}^2\right] \quad (16)$$

$$A_{m\_nc} = \left(2d_{ag} + 2b_e\right)^2 - 4d_{ag}^2 \quad (17)$$

$$A_{m\_nc} = 2\, d_{ag} b_e \quad (18)$$

where A_{m_nc} is the average macropore cross-sectional area of the noncylindrical porous block calculated from the previous 15 combinations of d_T and d_{ag}.

The average macropore cross-sectional area of the cylindrical porous block, A_{m_c}, is also needed in Equation 14 and is computed by setting $r_m = d_T$ (Figure 1, "Regularization"). The A_{m_nc} is demarcated from the matrix limit until the dashed red border (Figure 2). The noncylindrical porous block limits are denoted by the dashed red outer border in Figure 2, including the soil matrix.

3.1.2 | Macropore water flow

Macropore water flow for the cylindrical and noncylindrical porous block is needed in Equation 14 for the computation of the transformation factor. The macropore water flow was computed in the vertical direction for cylindrical and noncylindrical porous blocks. The macropore water flow for the noncylindrical porous blocks was computed from the dashed green outer border to the macropore-matrix boundary (Figure 2,_II–IV). The previously macropore water flow computed for all noncylindrical shapes was divided by two to represent the macropore water flow of the porous block (dashed red outer border to the macropore-matrix border). For more details, see the examples in the supplemental material.

The following conditions were imposed for macropore water flow: (a) laminar flow in the macropore, (b) the macropore has no interaction with the matrix (single-domain flow), and (c) the macropore is fully saturated.

The macropore water flow for the cylindrical porous block was computed analytically from the Hagen–

Poiseuille equation:

$$q_c = \frac{[\Delta p - \rho g \Delta x \sin(\theta)]\ \pi\ {r_m}^4}{8\eta\Delta x} \quad (19)$$

Where the q_c units are cubic meters per second, Δp is the pressure difference between the inlet and outlet boundary (Pa), θ is the angle between the horizontal and flow direction (degrees) where $\theta = -90°$ applies to vertical flow, and Δx is the length of the macropore (m).

The macropore water flow for noncylindrical porous blocks was computed analytically for the ring (Equation 20) (Papanastasiou, Georgiou, & Alexandrou, 1999), and rectangular slabs (Equation 21) (Spurk & Aksel, 2020) as follows:

$$q_{nc} = \frac{[\Delta P - \rho g \Delta x \sin(\theta)]\ \pi}{8\eta\Delta x}\left\{R_2^4 - d_{ag}^4 - \left[\frac{\left(R_2^2 - d_{ag}^2\right)^2}{\ln(R_2/d_{ag})}\right]\right\};\quad R_2 = d_{ag} + d_T \quad (20)$$

$$q_{nc} = \frac{4\ [\Delta P - \rho g \Delta x \sin(\theta)]\ {b_e}^3\ d_{ag}}{3\eta\Delta x} \times \left\{1 - \sum_{n=0}^{\infty} \frac{192}{(2n+1)^5\pi^5}\frac{b_e}{d_{ag}}\tanh\left[\frac{(2n+1)\ \pi d_{ag}}{2d_{ag}}\right]\right\} \quad (21)$$

where q_{nc} units are cubic meters per second, and Equation 21 was solved up to $n = 21$. The macropore water flow for hexagons and brick shapes was obtained through numerical simulation using COMSOL Multiphysics software in the vertical flow direction. Laminar flow conditions were imposed with no-slip boundary conditions at the walls for water at 20 °C. A no-flow condition was imposed in the macropore walls. Therefore, no interaction with the soil matrix was allowed (single-domain flow assumption). The following set of equations were solved using COMSOL:

$$\rho(\upsilon \cdot \nabla)\upsilon = \nabla \cdot \left\{-p\mathbf{I} + \eta\left[\nabla\upsilon + (\nabla\upsilon)^T\right]\right\} - \rho g \sin(\theta) \quad (22)$$

$$\rho\nabla \cdot (\upsilon) = 0 \quad (23)$$

where υ is the fluid velocity field (m s^{-1}), p is pressure (Pa), and $\mathbf{I}$ is the identity matrix. The macropore water flow for hexagon and brick shapes was finally obtained by integrating the fluid velocity field over the outlet area. A fine physics-controlled mesh was generated, and the numerical solutions were computed iteratively until stationary conditions were achieved.

In the flow equations (both analytical and numerical), the length of the macropore Δx was set as 5 cm, and the pressure head difference $\Delta p = 0$ Pa.

3.2 | Numerical solution error and Reynolds number

The numerical error of COMSOL simulations is computed by comparing COMSOL flow with the two available analytical solutions (Equations 20 and 21). The error was computed as a percentage:

$$\%\ \text{error} = 100\left|\frac{x - y}{x}\right| \quad (24)$$

where x is the flow computed by the analytical solution (Equations 20 and 21), and y is the flow computed by COMSOL numerically.

The assumption of laminar flow conditions was tested with the Reynolds number, Re, computed for rings and rectangular slabs as follows:

$$\text{Re} = \frac{\rho \upsilon_{avg} D_H}{\eta} \quad (25)$$

where $D_H = 4(A_R/\text{wet perimeter})$, v_{avg} is the average flow velocity (m s^{-1}) or the flow divided by the cross-sectional area of the macropore, and D_H is the hydraulic diameter (m).

4 | RESULTS

4.1 | Transformation factor

The relative macroporosity obtained from presuming cylindrical shapes (w_{f_c}) was always lower than the actual value for noncylindrical shapes (w_{f_nc}) (Figure 3).

The transformation factor, ξ, was almost constant with some small deviations in rings, hexagons, and bricks porous blocks (Figure 3). Recall that macropore water flow for both hexagons and bricks was obtained by numerical simulation, whereas analytical solutions were used for rings and rectangular slabs. The ξ appears to vary between 1.45 and 1.67 for all noncylindrical porous blocks. The deviations were mainly in the combinations generated with larger macropore widths and smaller effective aggregate width (d_{ag}).

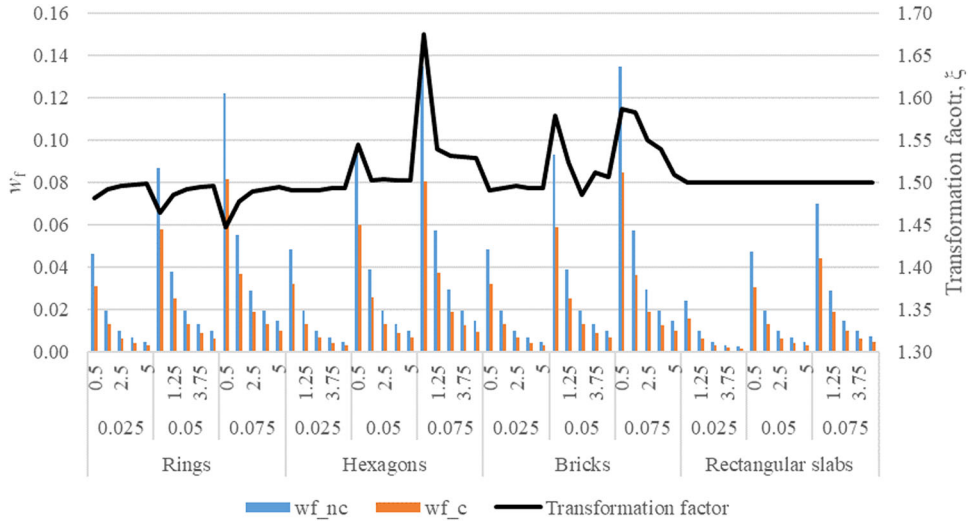

FIGURE 3 The transformation factor, ξ (black line), computed dividing the relative macroporosity for noncylindrical shapes, w_{f_nc}, by the relative macroporosity of cylindrical shapes, w_{f_c}. The lowermost *x* axis label is shape type, macropore width (cm), and effective aggregate width (cm)

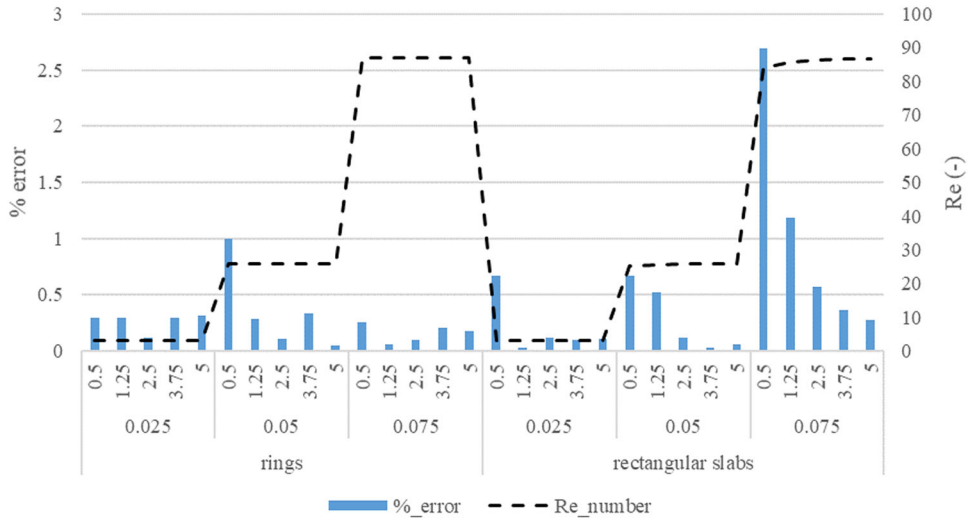

FIGURE 4 The left *y* axis shows the percentage error between the analytical and numerical computation of water flow for rings and rectangular slab shapes. The right *y* axis shows the Reynolds number (Re). The *x* axis shows (from bottom to top) shape type, macropore width (cm), and effective aggregate width (cm)

4.2 | Numerical solution and Reynolds number

The percentage error was higher for the smallest effective aggregate width for both rings and rectangular slabs shapes (Figure 4). Generally, the percentage error increases when the macropore width increases (Figure 4). The Reynolds number was lower than 100, and the correlation between the Reynolds number and the percentage error was 0.23, which is not significant.

5 | DISCUSSION

5.1 | Transformation factor

The transformation factor, ξ, is almost constant across noncylindrical porous blocks under different geometrical arrangements (Figure 3). Using the analytical solutions available for rings and rectangular slabs, we demonstrate that ξ is approximately equal to 1.5 (see the supplemental material). However, using the numerical solution for

hexagons and bricks, the solution for ξ seems to vary between 1.49 and 1.67 (Figure 3). This variation was produced by numerical error, which we computed for the ring and rectangular slabs using both analytical and numerical solutions (Figure 4). The most significant percentage numerical error occurs for the smallest effective aggregate width and the largest effective macropore width (Figure 4). For hexagonal and brick shapes, the largest deviations of ξ are of similar magnitudes as the percentage numerical errors previously mentioned for rings and rectangular slabs.

No turbulent flow conditions were observed in this analysis. The maximum Reynolds number computed was <100 for both rings and rectangular slabs shapes, whereas turbulent flow occurs at Reynolds number >1,000 (Jarvis, 2007). Consequently, ξ with a value of 1.5 applies to all the geometries analyzed under laminar flow conditions. The ξ of 1.5 applies for any macropore orientation (e.g., slope macropores). This conclusion can be seen by solving Equation 14 directly for rings or rectangular slabs where the pressure component $[\Delta P - \rho g \Delta x \sin(\theta)]$ is canceled (see the supplemental material).

5.1.1 | The effective macropore width

The effective macropore width (b_e) for field conditions may show a range of values. Only the minimum b_e in a pressure head range is found with the disk infiltrometer. Therefore, the actual value of the effective macropore width is a source of uncertainty. In Watson and Luxmoore (1986) database, the minimum radius ($2b_e$) was set to each pressure head range for the computation of w_f. The reason for using the minimum radius at each pressure head range was explained in Dunn and Phillips (1991). They concluded that for a macropore composed of different radius over depth, the narrowest part in the tube regulates the flow. The b_e can also be estimated by using the representative mean pore radius (Moret & Arrúe, 2007).

5.1.2 | Errors in the determination of the relative macroporosity and the number of macropores

The w_f obtained by presuming cylindrical porous block was, for all combinations, lower than the actual w_f for noncylindrical porous blocks. Therefore, the number of macropores is miscalculated if cylindrical shapes are always presumed, as is considered in the methodology of Watson and Luxmoore (1986). These outcomes reveal that for a more accurate determination of w_f by disk infiltrometers, the shape of the macropores should be considered. The macropore-matrix shape is usually not mentioned in reported disk infiltrometer studies (Nachabe, 1995; Schwärzel et al., 2011).

Because ξ was constant and equal to 1.5 between noncylindrical shapes, the actual noncylindrical shape is not relevant for computing w_f. The user needs to differentiate only between cylindrical and noncylindrical shapes under field conditions. In the case that the macropore-matrix shape cannot be recognized over the total surface area of infiltration, a cylindrical shape should be assumed.

5.1.3 | Errors in the determination of the effective aggregate width

The miscalculation of w_f presuming cylindrical shapes propagates as an error into the effective aggregate width, d_{ag}. The ratio between the actual value for d_{ag} and the miscalculated value is proportional to 1/ξ (see Equations 7 and 8). Two primary sources of error can be produced when computing d_{ag}. The first error relates to choosing the correct macropore-matrix shape under field conditions but without applying the transformation factor. The second error is mismatching the shape under field conditions. In the second case, it is assumed that the transformation factor was applied correctly.

Let us consider a field condition with rectangular slab macropores, where $b_e = 0.05$ cm, $w_{f\_c} = 0.004$, $\xi = 1.5$, and, using Equation 8, $d_{ag} = 8.28$ cm. The first error (not applying ξ in Equation 8) overestimates the final value of d_{ag} by 50% ($d_{ag} = 12.45$ cm). The second error of choosing a wrong macropore-matrix shape underestimates d_{ag} by 82% ($d_{ag} = 1.48$ cm) when cylindrical macropores (Equation 6) are used instead of rectangular slabs (Equation 8). In the case of choosing rings, hexagons, or bricks instead of the actual rectangular slab shape, the value of d_{ag} is overestimated a 100% ($d_{ag} = 16.59$ cm). The overestimation of d_{ag} is related to larger macropore spacings. Smaller distances between the macropore wall and the center of the matrix imply less preferential flow. Distances of 0.1 cm are considered close to equilibrium (Gerke & van Genuchten, 1993a) or one domain flow (Larsson & Jarvis, 1999). Therefore, it is relevant to choose the correct macropore-matrix shape under field conditions for d_{ag}. However, if we denoted rings, hexagons, and bricks shapes as even-sided polygons or "closed shapes," practitioners need to differentiate only between cylindrical, "closed shapes," and rectangular slabs for d_{ag}. Hence, it is not necessary to know the actual "closed shape" under field conditions, which is convenient. Previous conclusions are different from the one for w_f, where the user only needs to differentiate between cylindrical and noncylindrical shapes.

5.2 | Physical assumptions in the estimation of the transformation factor

The ξ computed for noncylindrical porous blocks is based on simplifying assumptions of the physical processes for macropore water flow, which could deviate from the actual flow at field conditions. Quasi-steady-state and one-dimensional flow conditions are a requirement for the developed methodology. Quasi-steady-state conditions are commonly challenging to achieve, especially for smaller pressure heads values at the base of the disk (Šimůnek, Wendroth, & van Genuchten, 1999). Watson and Luxmoore (1986) proposed to saturate the soil with a double ring initially and then place the disk infiltrometer to reduce the time it takes to reach a quasi-steady state. A one-dimensional flow condition can be achieved by increasing the diameter of the disk infiltrometer. A larger diameter will increase the vertical hydraulic head gradient relative to the horizontal hydraulic head gradient (Šimůnek, Angulo-Jaramillo, Schaap, Vandervaere, & van Genuchten, 1998; Wooding, 1968).

5.3 | Mixed shapes

Macropore-matrix shapes are likely mixed under field conditions. In that case, we advise that the same procedure should be followed for each shape independently. However, the final w_f value to be used in the models should be multiplied by a weight factor corresponding to their relative abundance over the total surface area of infiltration and the differences in water flow:

$$w_f = \phi_c\, w'_{f\_c} + (1 - \phi_c)\,\xi w'_{f\_c} \tag{26}$$

$$\phi_c = \left[1 + \frac{q_{nc}}{q_c}\left(\frac{1}{\phi_{Ac}} - 1\right)\right]^{-1};\ \phi_{Ac}\ ]0,1] \tag{27}$$

where ϕ_c is the proportion of the relative macroporosity corresponding to cylinders, the subscripts "n" and "nc" are cylindrical and noncylindrical shapes, w'_{f_c} is the relative macroporosity presuming that cylindrical macropores transport all the infiltrated water by disk infiltrometer (computed following Case 1 in Section 2), and ϕ_{Ac} is the proportion of cylindrical porous blocks over the total number of porous blocks (including cylindrical and noncylindrical shapes). The value of ϕ_{Ac} is subjectively chosen by the practitioner under field conditions and is an open subject for future research.

Each relative macroporosity can be used to compute d_{ag} for mixed shapes in a similar way. Equation 26 is for two macropore-matrix shapes, including a cylindrical macropore and a noncylindrical macropore. Equation 26 can be expanded to more macropore combinations. More details about the construction of Equations 26 and 27 are given in the supplemental material.

In Equations 27, the macropore water flow for the cylindrical (q_c) and noncylindrical (q_{nc}) shape is needed. This computation can be done by using the analytical solutions for cylinder (Equation 19), ring (Equation 20), and rectangular slab (Equation 21). In the case that hexagon or brick shapes are mixed with cylinders, the user might use numerical solutions. However, following the same construction of shapes performed in this research for the transformation factor, the macropore water flow through hexagons can be approximated as 3.5 times the one for rectangular slabs. In the case of bricks, the transformation factor is 4.0 times the one for rectangular slabs.

Follow-up studies can be conducted to implement a more precise pore-scale model of the macropore water flow for non-cylindrical porous blocks. Under field conditions, the flow can be in rivulets or films (Germann, Helbling, & Vadilonga, 2007; Nimmo, 2010) or even turbulent (Beven & Germann, 2013; Chen & Wagenet, 1992; Jarvis, 2007), especially for bigger diameters (or width) of macropores (Germann, 1987). We anticipate that if the macropore water flow for noncylindrical shapes is different from laminar, the transformation factor should increase from 1.5. In follow-up studies, we advise that the macropore water flow for the transitional cylindrical porous block should be kept as a fully saturated cylindrical macropore shape under laminar flow conditions, to maintain the physical meaning of ξ.

The user should be aware that this methodology is an initial approximation for d_{ag} and w_f presuming nearly quasi-steady-state and one-dimensional flow conditions. Commonly, three-dimensional flow is expected under field conditions when the disk infiltrometer is applied (Stewart, Abou Najm, Rupp, & Selker, 2016).

6 | CONCLUSIONS

Disk infiltrometers have been typically used to obtain the relative macroporosity (w_f) and the number of macropores in the field, under the presumption of cylindrical macropore shapes. We generalize the computation of w_f with disk infiltrometers by introducing a transformation factor, ξ, derived from pore-scale modeling. The ξ was computed, accounting for differences in macropore area and water flow between the actual shape (ring, hexagon, brick, and rectangular slab) and the transitional cylindrical shape (cylindrical macropores). Macropore water flow was solved analytically for the cylindrical, ring, and

rectangular slab shapes. Macropore water flow for hexagon and brick shapes was solved numerically using COMSOL Multiphysics software. The ξ appeared to be constant and equal to 1.5 for all the noncylindrical shapes analyzed.

An explicit mathematical and geometrical relation was presented for w_f, and the effective aggregate width (d_{ag}) for all the studied macropore-matrix shapes. The computation of ξ for w_f allows the computation of d_{ag} from disk infiltrometer data for noncylindrical geometries. The use of ξ in obtaining d_{ag} and w_f is an exact solution under the physical assumptions used for macropore water flow in this study. We derived an equation for computing w_f for soils containing mixed macropore-matrix shapes. The user needs to know the relative abundance of cylindrical porous blocks over the total number of porous blocks below the surface area of infiltration.

The current methodology can be applied to previous databases of disk infiltrometer data. Three conditions are required for the use of this methodology: (a) there should be quasi-steady-state conditions during the disk infiltrometer measurement, (b) the macropore-matrix shape should be known, and (c) the water displaced from the disk infiltrometer reservoir should be measured for at least two pressure head ranges, always including a measurement at zero pressure head.

Both w_f and d_{ag} are input parameters for several dual-permeability models, such as HYDRUS, SWAP, and MACRO. The d_{ag} is used in both water flow and chemical transport components of currently available models and is a very sensitive parameter to water flow, water content over depth, and pesticide leaching (Gerke & van Genuchten, 1993a; Jarvis & Larsbo, 2012; Larsbo, Roulier, Stenemo, Kasteel, & Jarvis, 2005; Tiktak et al., 2012). To our knowledge, this is the first study that has developed an independent estimate for d_{ag} under field conditions for different geometries with disk infiltrometers. Therefore, the findings of this investigation may have substantial implications on the modeling of water flow and solute transport in soil profiles, and the leaching of agrochemicals and other pollutants to groundwater and surface water. This methodology can be applied to find an initial estimate of d_{ag} and w_f for risk assessment problems and regional studies, or for use as an initial value for fitting parameters in inverse models.

ACKNOWLEDGMENTS

This work was funded by the Comisión Nacional de Investigación Científica y Tecnológica, CONICYT PFCHA/Doctorado Becas Chile/2015-72160322 (grant). D.W.S.T acknowledges the financial support of the Re-USe of Treated effluent for agriculture (RUST) project of the Netherlands Organisation for Scientific Research (NWO).

CONFLICT OF INTEREST

The authors declare no conflict of interest.

ORCID

C. A. Faúndez Urbina https://orcid.org/0000-0003-4925-5277

REFERENCES

Arora, B., Mohanty, B. P., & McGuire, J. T. C. W. (2011). Inverse estimation of parameters for multidomain flow models in soil columns with different macropore densities. *Water Resources Research*, *47*(4). https://doi.org/10.1029/2010wr009451

Beven, K., & Germann, P. (2013). Macropores and water flow in soils revisited. *Water Resources Research*, *49*, 3071–3092. https://doi.org/10.1002/wrcr.20156

Chen, C., & Wagenet, R. J. (1992). Simulation of water and chemicals in macropore soils Part 1. Representation of the equivalent macropore influence and its effect on soil water flow. *Journal of Hydrology*, *130*, 105–126. https://doi.org/10.1016/0022-1694(92)90106-6

Dunn, G. H., & Phillips, R. E. (1991). Equivalent diameter of simulated macropore systems during saturated flow. *Soil Science Society of America Journal*, *55*, 1244–1248. https://doi.org/10.2136/sssaj1991.03615995005500050008x

Gardenas, A. I., Simunek, J., Jarvis, N., & van Genuchten, M. Th. (2006). Two-dimensional modelling of preferential water flow and pesticide transport from a tile-drained field. *Journal of Hydrology*, *329*, 647–660. https://doi.org/10.1016/j.jhydrol.2006.03.021

Gerke, H. H., & van Genuchten, M. Th. (1993a). A dual-porosity model for simulating the preferential movement of water and solutes in structured porous media. *Water Resources Research*, *29*, 305–319. https://doi.org/10.1029/92wr02339

Gerke, H. H., & van Genuchten, M. Th. (1993b). Evaluation of a first-order water transfer term for variably saturated dual-porosity flow models. *Water Resources Research*, *29*, 1225–1238. https://doi.org/10.1029/92wr02467

Gerke, H. H., & van Genuchten, M. Th. (1996). Macroscopic representation of structural geometry for simulating water and solute movement in dual-porosity media. *Advances in Water Resources*, *19*, 343–357. https://doi.org/10.1016/0309-1708(96)00012-7

Germann, P. F. (1987). The three modes of water flow through a vertical pipe. *Soil Science*, *144*, 153–154.

Germann, P., Helbling, A., & Vadilonga, T. (2007). Rivulet approach to rates of preferential infiltration. *Vadose Zone Journal*, *6*, 207–220. https://doi.org/10.2136/vzj2006.0115

Hu, Y., Feng, J., Yang, T., & Wang, C. (2014). A new method to characterize the spatial structure of soil macropore networks in effects of cultivation using computed tomography. *Hydrological Processes*, *28*, 3419–3431. https://doi.org/10.1002/hyp.9902

Jarvis, N. J. (2007). A review of non-equilibrium water flow and solute transport in soil macropores: Principles, controlling factors and consequences for water quality. *European Journal of Soil Science*, *58*, 523–546. https://doi.org/10.1111/j.1365-2389.2007.00915.x

Jarvis, N., & Larsbo, M. (2012). MACRO (v5.2): Model use, calibration, and validation. *Transactions of the ASABE*, *55*, 1413–1423. https://doi.org/10.13031/2013.42251

Köhne, J. M., Köhne, S., & Gerke, H. H. (2002). Estimating the hydraulic functions of dual-permeability models from bulk soil data. *Water Resources Research*, *38*, 11–26. https://doi.org/10.1029/2001wr000492

Köhne, J. M., & Mohanty, B. P. C. W. (2005). Water flow processes in a soil column with a cylindrical macropore: Experiment and hierarchical modeling. *Water Resources Research*, *41*(3). https://doi.org/10.1029/2004wr003303

Larsbo, M., Roulier, S., Stenemo, F., Kasteel, R., & Jarvis, N. (2005). An improved dual-permeability model of water flow and solute transport in the vadose zone. *Vadose Zone Journal*, *4*, 398–406. https://doi.org/10.2136/vzj2004.0137

Larsson, M. H., & Jarvis, N. J. (1999). Evaluation of a dual-porosity model to predict field-scale solute transport in a macroporous soil. *Journal of Hydrology*, *215*, 153–171. https://doi.org/10.1016/S0022-1694(98)00267-4

Moret, D., & Arrúe, J. L. (2007). Characterizing soil water-conducting macro and mesoporosity as influenced by tillage using tension infiltrometry. *Soil Science Society of America Journal*, *71*, 500–506. https://doi.org/10.2136/sssaj2006.0128

Nachabe, M. H. (1995). Estimating hydraulic conductivity for models of soils with macropores. *Journal of Irrigation and Drainage Engineering*, *121*, 95–102. https://doi.org/10.1061/(ASCE)0733-9437(1995)121:1(95)

Nimmo, J. R. (2010). Theory for source-responsive and free-surface film modeling of unsaturated flow. *Vadose Zone Journal*, *9*, 295–306. https://doi.org/10.2136/vzj2009.0085

Papanastasiou, T., Georgiou, G., & Alexandrou, A. N. (1999). *Viscous fluid flow*. Boca Raton, FL: CRC Press.

Perroux, K. M., & White, I. (1988). Designs for disc permeameters. *Soil Science Society of America Journal*, *52*, 1205–1215.

Schwärzel, K., Carrick, S., Wahren, A., Feger, K.-H., Bodner, G., & Buchan, G. (2011). Soil hydraulic properties of recently tilled soil under cropping rotation compared with two-year pasture. *Vadose Zone Journal*, *10*, 354–366. https://doi.org/10.2136/vzj2010.0035

Scorza Júnior, R. P., Jarvis, N. J., Boesten, J. J. T. I., van der Zee, S. E., & Roulier, S. (2007). Testing MACRO (version 5.1) for pesticide leaching in a Dutch clay soil. *Pest Management Science*, *63*, 1011–1025. https://doi.org/10.1002/ps.1434

Scorza Júnior, R. P., Smelt, J. H., Boesten, J. J. T. I., Hendriks, R. F. A., & van der Zee, S. E. A. T. M. (2004). Preferential flow of bromide, bentazon, and imidacloprid in a Dutch clay soil. *Journal of Environmental Quality*, *33*, 1473–1486. https://doi.org/10.2134/jeq2004.1473

Šimůnek, J., Angulo-Jaramillo, R., Schaap, M. G., Vandervaere, J.-P., & van Genuchten, M. Th. (1998). Using an inverse method to estimate the hydraulic properties of crusted soils from tension-disc infiltrometer data. *Geoderma*, *86*, 61–81. https://doi.org/10.1016/S0016-7061(98)00035-4

Šimůnek, J., Wendroth, O., & van Genuchten, M. Th. (1999). Estimating unsaturated soil hydraulic properties from laboratory tension disc infiltrometer experiments. *Water Resources Research*, *35*, 2965–2979. https://doi.org/10.1029/1999wr900179

Spurk, J. H., & Aksel, N. (2020). *Fluid mechanics* (3rd ed.). Cham, Switzerland: Springer. https://doi.org/10.1007/978-3-030-30259-7

Stewart, R. D., Abou Najm, M. R., Rupp, D. E., & Selker, J. S. (2016). Modeling multidomain hydraulic properties of shrink-swell soils. *Water Resources Research*, *52*, 7911–7930. https://doi.org/10.1002/2016WR019336

Tiktak, A., Hendriks, R. F. A., Boesten, J. J. T. I., & van der Linden, A. M. A. (2012). A spatially distributed model of pesticide movement in Dutch macroporous soils. *Journal of Hydrology*, *470–471*, 316–327. https://doi.org/10.1016/j.jhydrol.2012.09.025

Tiktak, A., Hendriks, R. F. A., & Boesten, J. J. T. I. (2012). Simulation of movement of pesticides towards drains with a preferential flow version of PEARL. *Pest Management Science*, *68*, 290–302. https://doi.org/10.1002/ps.2262

Urbina, C. A. F., van Dam, J. C., Hendriks, R. F. A., van den Berg, F., Gooren, H. P. A., & Ritsema, C. J. (2019). Water flow in soils with heterogeneous macropore geometries. *Vadose Zone Journal*, *18*(1). https://doi.org/10.2136/vzj2019.02.0015

Van den Berg, F., Gottesbüren, B., Hammel, K., Jarvis, N., & Poot, A. (2014). *Drainage models and macroporous soils: Report of a SETAC workshop*. Paper presented at a Society of Environmental Toxicology and Chemistry Workshop, Vienna.

van Schaik, N. L. M. B., Hendriks, R. F. A., & van Dam, J. C. (2010). Parameterization of macropore flow using dye-tracer infiltration patterns in the SWAP model. *Vadose Zone Journal*, *9*, 95–106. https://doi.org/10.2136/vzj2009.0031

Watson, K. W., & Luxmoore, R. J. (1986). Estimating macroporosity in a forest watershed by use of a tension infiltrometer. *Soil Science Society of America Journal*, *50*, 578–582. https://doi.org/10.2136/sssaj1986.03615995005000030007x

Wooding, R. A. (1968). Steady infiltration from a shallow circular pond. *Water Resources Research*, *4*, 1259–1273. https://doi.org/10.1029/WR004i006p01259

Zhang, J., Xu, Z., Li, F., Hou, R., & Ren, Z. (2017). Quantification of 3D macropore networks in forest soils in Touzhai valley (Yunnan, China) using X-ray computed tomography and image analysis. *Journal of Mountain Science*, *14*, 474–491. https://doi.org/10.1007/s11629-016-4150-9

SUPPORTING INFORMATION

Additional supporting information may be found online in the Supporting Information section at the end of the article.

How to cite this article: Urbina CAF, van Dam J, van den Berg F, Ritsema CJ, Tang DWS. Determination of the relative macroporosity and the effective aggregate width for different macropore geometries with disk infiltrometers. *Vadose Zone J*. 2020;19:e20048. https://doi.org/10.1002/vzj2.20048